JOURNAL OF AIRCRAFT
Vol. 30, No. 6, Nov.–Dec. 1993

Response of Helicopter Blades to a Sharp Collective Increase

Y. Hecht* and O. Rand†
Technion—Israel Institute of Technology, Haifa 32000, Israel

This article presents a theoretical investigation of the response of helicopter blades to a sharp collective increase in hover. The modeling deals with both main aspects of the problem: 1) the spanwise distribution of the unsteady loads, and 2) the corresponding structural dynamic response of the elastic blades and the rotor-fuselage system as a whole. The aerodynamic loads distribution is calculated by the definition and the determination of the spanwise distribution of the aerodynamic equivalent mass, which is responsible for the time-dependent development of the velocity induced by the trailing vortices. The structural modeling is based on the finite element approach, and the equations of motion are derived using Lagrange's equations. Due to the sharp changes in time, all terms containing time derivatives are retained in the equations which results in highly nonlinear expressions. A study to identify and quantify the role and the sensitivity of a variety of parameters has been carried out.

Introduction

ONE of the maneuvers required in a typical mission of a modern attack helicopter is a "bob-up" climbing from hover in order to be located in minimal time in an upper position. Such a maneuver is achieved mainly by a rapid increase of the collective pitch angle. The helicopter response in this case is complex, and detailed analysis is required in order to enable suitable design of rotor systems that will be capable of sustaining sharp loading changes which are forced by the rapid collective increase.

The earliest and well-known published experimental and theoretical investigation of the response of helicopter rotor blades to a rapid collective pitch increase is that of Carpenter and Fridovich.[1] In this report, experimental data of blades undergoing sharp collective changes up to 200 deg/s are presented along with correlation with an analytic model. The latter was based on the apparent mass of the air associated with the acceleration of an impervious disc normal to its plane, and includes some correction constants. The dynamic analysis is based on the assumption that the blades were infinitely stiff. This work served as a basis for comparison of advanced models that will be discussed later.

The problem of predicting the aerodynamic loads in the case of a sharp collective change may be viewed as a special case of the general problem of predicting the aerodynamic loads on helicopter blades. In principle, any time stepping numerical scheme such as those which are based on the vortex theory[2] should be suitable for calculating the loads development due to a sharp collective change. Examples for such schemes are Refs. 3 and 4. Segel[3] presented one of the earliest vortex wake modelings, while Quackenbush[4] presents the application of an advanced free-wake analysis to ramp inputs of collective and comparisons with the experimental results of Ref. 1. Reference 4 concentrated on the relative low-rate commands where reasonable correlation with experiments may be obtained by dealing only with the aerodynamic aspect. It is beyond the scope of this article to review the wide range of additional methods developed for predicting blades aerodynamic loads, and therefore, the following discussion concentrates on the specific case of the loads that result from a sharp collective increase in hover which exhibits some unique characteristics. Moreover, since the dynamic analyses of elastic blades require a large number of repeated calculations of aerodynamic loads, there is a need to adopt approximate formulations. Thus, the following discussion will concentrate on such approximate models, while a detailed review of the literature may be found in Ref. 5.

Before preceding to the description of the relevant studies, it should be mentioned that in hover, rapid collective increase is similar to vertical gust loading.[6] However, careful examination shows that these problems are different from both aerodynamic and structural dynamic points of view. In both cases the effective angle of attack grows rapidly, however, in the case of gust loading, the wake vortices are also pushed down by the gust, while in the case of rapid collective pitch increase, the vortices downwards motion is developed gradually by the high-intensity vortices that are added to the flowfield as a result of the higher loads which are developed over the blades. From a structural dynamics point of view, the product of inertia which is generated by the pitch angle is absent in gust loading, and therefore, the dynamic couplings are reduced in such cases.

Rebont et al.[7] presented an experimental investigation for the case of descending axial flight and correlated the results with theoretical predictions based on a model similar to the one presented in Ref. 1. They concluded that a double value for the apparent mass yields better agreement with experimental results in this case.

Pitt and Peters[8] proposed the model known as "dynamic inflow" which is based on analytic solution of the flowfield around the rotor disc, while the pressure distribution is described by a special family of known functions. This model relates the aerodynamic perturbation in thrust, roll moment, and pitch moment to the induced flow distribution by a linear first-order system of equations. For the axial flight region, it has been concluded that the apparent mass terms for the simplest pressure distribution are identical to those obtained for an impermeable disc, but these values vary significantly with the pressure distribution. It has also been recommended to develop a dynamic inflow model that will also account for wake contraction, finite number of blades, and reduced frequency effects.

Chen and Hindson[9] reviewed the influence of dynamic inflow on the helicopter vertical response. They compared the models presented in Refs. 1 and 8, and concluded that there is reasonable agreement between calculated results of these models and experiments, and that the induced velocity and initial conditions play an important role. They also indicated that the model presented in Ref. 8 tends to produce more

Received Sept. 25, 1991; revision received June 17, 1992; accepted for publication Aug. 20, 1992.

*Graduate Student, Faculty of Aerospace Engineering.
†Senior Lecturer, Faculty of Aerospace Engineering.

oscillatory response, and that taking into account the changes in the rotor speed may improve the correlation.

Generally, the above investigations show that unsteady aerodynamic effects play an important role. However, it should be emphasized that the above models do not include the flexibilities of the blades which may be important in many cases, in particular for full-scale blades (as opposed to experimental blades which are relatively stiff). Moreover, in the axial flight region, the above approximate models are concentrated on the prediction of integral quantities (averaged induced velocity, rigid flap angle, and thrust). Thus, time-dependent development of the induced velocity distribution along the span is not dealt with. This distribution appears essential for a realistic evaluation of the lift distribution as required during the determination of elastic blades response.

From a structural point of view, the literature contais various models that are capable of representing elastic blades.[1] In the present case of sharp changes in time, adoption of the finite element approach seems to be inevitable due to the need to enable a time-dependent simulation of dynamic response whch contains a vast range of a priori unknown frequencies that depend on the shape and rate of the specific command.

The task of the present model is to formulate an approximate analytical model which will be capable of simulating the time history of the spanwise distribution of the induced velocity and the structural dynamic response of elastic blades and the rotor/fuselage system. The proposed mathematical formulation is capable of examining a variety of phenomena imposed by a rapid collective increase in hover, and therefore, provides a better insight into the physical phenomenon.

Analysis

Aerodynamic Loads

The present formulation is based on separating the problem into two regions: 1) the external field and 2) the internal field. This separation is based on the traditional description of the flowfield mechanisms by discrete vortex lines. From this point of view, it is possible to show that a substantial part of the induced velocity over the blade is contributed by the trailing vortices which are created by the spanwise variations of the bound circulation. These vortices are located at all times in the blade's vicinity and their influence is three-dimensional (i.e., vortices which are shed from a certain cross section induce velocity over other cross sections and over other blades as well). Thus, the trailing vortices are suitable to be considered as the external field in which the interaction between the blades and their wakes is also taken into account. Based on the vortex theory, the influence of the trailing vortices is determined in this article by a first-order extension of the classical "blade-element-momentum" theory.

The shed vortices which are created by the time variations of the bound circulation are characterized, in contrast with the trailing vortices, by relatively short influence distances and are therefore suitable to be taken into account by two-dimensional considerations as the internal field. Thus, an unsteady two-dimensional analysis is carried out in the internal field for each cross section along the blade span. For that purpose, the formulation presented by Dinyavari and Friedmann[10] is adopted and supplemented by noncirculatory terms and quasisteady compressibility corrections. This formulation enables the calculation of the loads using two-state variables which are obtained by the time history of the normal velocity at the three-quarter-chord point. This velocity contains also the velocity induced by the trailing vortices of the external field, while the shed vortices are consistently included in the loads expressions.

External Field Formulation

As mentioned above, the present analysis is based on the extension of the classical blade-element-momentum theory.[2] By momentum considerations for a control volume V, which is defined by a ring in the rotor disc and the streamlines that pass along its internal and external circumference, it is possible to express the thrust vector generated over the ring area in the disc plane as

$$\bar{T} = \frac{\partial}{\partial t}\int\int_V\int \rho\bar{u}\,\mathrm{d}V + \int_S\int \bar{u}(\rho\bar{u}\cdot\hat{n}\,\mathrm{d}S) \qquad (1)$$

where ρ is the fluid density, $\bar{u}$ is the velocity vector at each point in the control volume, t stands for time, $\hat{n}$ is a unit vector normal to the control volume surface (positive when directed outside), and S is the control volume surface. Clearly, the steady momentum theory does not account for the first term in Eq. (1). As shown in Ref. 2, it is possible to write the steady contribution of the above control volume [based on the second term in Eq. (1)] as

$$\mathrm{d}T_M = 4\pi\rho r v(V_c + v)\,\mathrm{d}r \qquad (2)$$

where $\mathrm{d}T_M$ is the thrust over a ring of width $\mathrm{d}r$ located at r (positive when directed upwards), v is the induced velocity at r (positive when directed downwards), and V_c is the rotor climb velocity (positive when directed upwards).

At this stage, the introduction of the first (unsteady) term in Eq. (1) is studied. It is clear that this unsteady term represents thrust that has been created by accelerating the air around the disc, and therefore, its contribution might be significant where sharp time changes in thrust take place. In addition, it is clear that the air is accelerated differently at various locations in the disc vicinity. On top of that, representing the flowfield around the disc by vortex filaments shows that is impossible to consider each ring separately (as opposed to the steady case for large enough numbers of blades[11]). Also, the classical assumptions of the momentum theory that led to Eq. (2) are not necessarily justified in this unsteady case.

In order to develop the present approximation it was assumed that there is a time-independent constant that relates the rate of induced velocity change at a certain radial location over the disc to the unsteady part of the thrust per unit length created at the same location. Consequently, it is possible to formulate the contribution of each ring to the overall thrust by

$$\frac{\mathrm{d}T_M}{\mathrm{d}r} = 4\pi\rho r v(V_c + v) + m_{(r)}\dot{v} \qquad (3)$$

where m will be referred to as the "equivalent mass" and is assumed to be a function of the ring radial location only, and has a dimension of mass per unit length. As shown, the unsteady part has not been changed [see Eq. (2)]. Note that this expression is similar to the classical "global" expression given in Ref. 1 which associates the overall induced velocity and thrust. Once the assumption made in Eq. (3) is proven to be apropriate, it has the following advantages:

1) It associates the induced velocity of each ring with its own thrust only.

2) It enables clear identification of the unsteady and steady contributions and therefore may be reduced directly to the steady case.

3) It preserves the basic structure of the exact equation [Eq. (1)].

It should be emphasized that the equivalent mass is associated with the external field time delays and it is different from the apparent mass which is usually associated with the noncirculatory terms in two-dimensional unsteady analysis (which may or may not be included in the two-dimensional formulation of the internal field). Moreover, the external field/internal field concept yields an external field of relatively low velocities where the present incompressible concept of equivalent mass is justified. However, in the internal field, com-

pressible, unsteady two-dimensional analysis should be performed.

The most critical assumption made in Eq. (3) is that $m(r)$ is not a function of time, which also states that it is independent of the command shape (or the circulation history). The justification of the above assumptions and the determination of $m(r)$ are dealt with in the following.

At this stage it is possible to examine in what way the above-mentioned equivalent mass appears in the aerodynamic load expressions. First, the thrust created by a bound vortex element is given by

$$dT_e = \rho\Omega r\Gamma\, dr \tag{4}$$

where dT_e is a thrust element, Ω is the rotor angular velocity, N_B is the number of blades, and Γ is the bound vortex at radius r. Equating Eqs. (3) and (4) gives

$$4\pi rv(V_c + v) + m\dot{v} = \Omega r\Gamma b \tag{5}$$

On the other hand, the bound vortex strength as a function of the time-dependent induced velocity may be determined by any, either steady or unsteady, two-dimensional airfoil theory. For example, in the simplest case of the steady blade-element strip theory, Γ is given by

$$\Gamma = \tfrac{1}{2}\Omega rca[\theta - (v/\Omega r)] \tag{6}$$

where a is the lift curve slope, c is the blade chord, and θ is the blade local pitch angle. Combining Eq. (5) with Eq. (6) by eliminating Γ, yields an equation where the unknowns are $v(r, t)$ and $m(r)$. Clearly, in the steady case, this equation defines $v(r)$, however, additional information is required in the unsteady case. This information cannot be obtained from the momentum theory or from the blade-element theory or from their combination, but it may be acquired from the combination of the vortex theory with the momentum theory. Therefore, a consistent way for determining $m(r)$, which is based on the vortex theory, is dealt with next.

In order to calculate the time changes in the induced velocity while using the vortex theory, a time-stepping numerical scheme that will enable the calculation of the induced velocity over each cross section at any moment should be utilized. Using this velocity, the vorticity that generates vortex elements which are added in each time step to the flowfield is calculated (within the internal field), and all other elements in the flowfield are "shifted" properly. For the sake of clarification it will be assumed that such a scheme has been applied to a given $\Gamma(r, t)$, the corresponding values of the induced velocity $\bar{v}_V(r, t)$ were obtained, and it is desired to find the corresponding values of $m(r)$. Assuming that the induced velocity at the beginning of the process is v_0, Eqs. (5) and (6) may be integrated in the following form:

$$v = \frac{1}{m}\int_0^t \left[\frac{1}{2}N_B\Omega^2 r^2 ca\left(\theta - \frac{v}{\Omega r}\right) - 4\pi rv(V_c + v)\right] dt + v_0 \tag{7}$$

Note that Eq. (6) could have been replaced by any other (either steady or unsteady) relation that connects the time-dependent induced velocity and the time-dependent circulation. Now, it is possible to set the requirement that the sum of the squares of the discrepancies between the induced velocity which is obtained from Eq. (7) and that which is obtained by the vortex theory will be minimal along a given time interval t_0, namely

$$\text{minimize over } m \qquad \int_0^{t_0} (v - \bar{v}_V)^2\, dt \tag{8}$$

The values of $m(r)$ are obtained from the above minimization which is carried out for each cross section. As will be shown in the following study, $m(r)$ exhibits low sensitivity to most of the relevant parameters, and therefore, a priori values of $m(r)$ may be used in many of the practical cases. Clearly, once $m(r)$ is known, the induced velocity time history may be directly calculated by Eq. (5) for any given time-dependent circulation. Compared with the robust numerical vortex-theory scheme, the required computational effort is negligible in this case.

Equivalent Mass Characteristics

To demonstrate some characteristics of the above formulation, a numerical scheme based on the vortex theory is required. In this article, a helical wake model with varying spacings has been used. If needed, this model can be replaced by any other wake model. The output of this code is the distribution of the induced velocity at each moment as function of the blade span. In what follows, the results of a sequence of checks are presented. In these cases, the rotor is assumed not to produce thrust at $t < 0$. At $t \geq 0$, thrust is starting to be created by various command shapes.

The purpose of the first check is to show that the value for the equivalent mass which has been obtained from the minimization process [Eq. (8)] permits the approximation of the induced velocity time history. The results of this check using a step increase of circulation are shown in Fig. 1. As shown, the development of the induced velocity as function of time, which is obtained by using the above equivalent masses, yields a good approximation of the vortex theory result. Using the same values of the equivalent mass, the induced velocity development in the case of double-step variation of the circulation was examined and the satisfactory correlation is shown in Fig. 2.

The purpose of the next check is to find the sensitivity of the equivalent mass values to the command shape characteristics. Consequently, the mass values which were obtained by different time histories of bound circulation initiated from zero at $t = 0$ and terminated at the same final values were examined (see Fig. 3). Generally, it may be stated that the equivalent mass distribution exhibits only low sensitivity to the command shape characteristics.

Next, the sensitivity of the equivalent mass to changes in the rotor number of blades is studied. For that purpose, values which were obtained by a step function for a different number

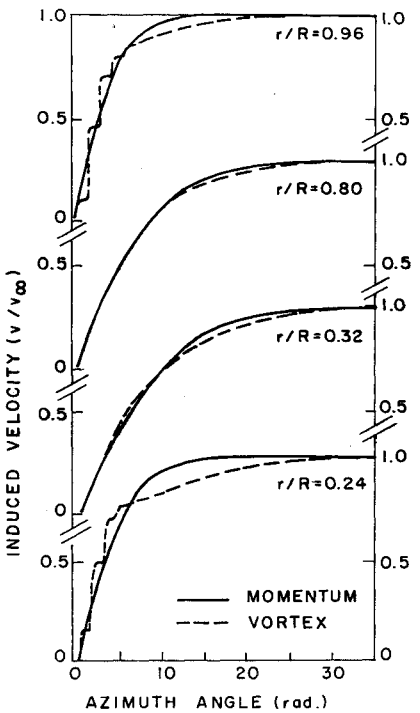

Fig. 1 Induced velocity development for a step function in circulation.

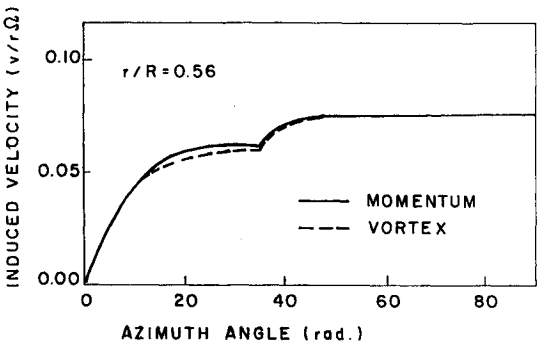

Fig. 2 Induced velocity development for a double-step command.

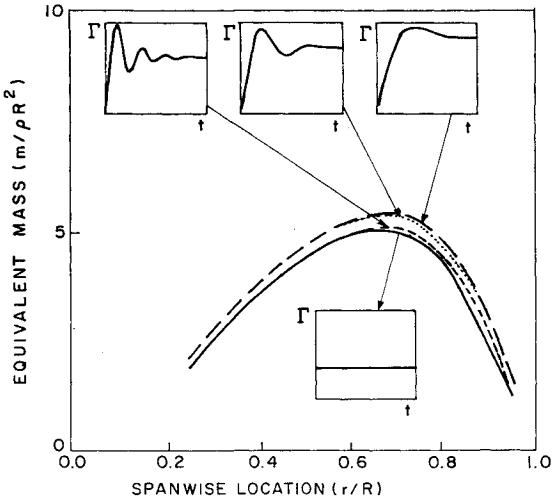

Fig. 3 Equivalent mass values for different command shapes.

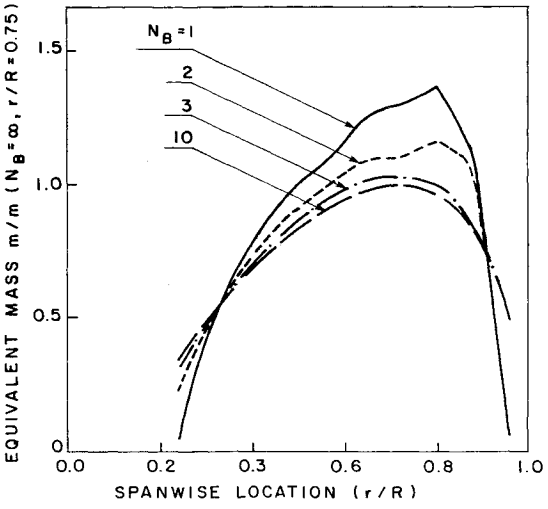

Fig. 4 Equivalent mass values for a different number of blades.

of blades are presented in Fig. 4. As shown, the spanwise distribution of the equivalent mass becomes sharper as the number of blades is decreased. Thus, it may be concluded that for rotors having three blades or more, the number of blades has only a limited influence on the equivalent mass values and an asymptotic convergence is obtained as the number of blades is increased. It should be noted that integrating the distributed mass along the blade span for the case of a large number of blades yields a value which is larger by 10% than the value used in Ref. 1 for an impervious disc.

The sensitivity of the equivalent mass values to different end values of bound circulation is examined next. The mass values obtained by step function commands with zero initial conditions and various end values of circulation (75, 100, and 150% of the nominal case) are presented in Fig. 5. As shown, the circulation end values have negligible influence.

To study the influence of the values of the induced velocity and the bound vorticity at the starting moment ($t = 0$), the circulation end values of a number of step function commands were kept constant while the initial values were 0, 17, 33, 50, and 67% of the end value. The results are presented in Fig. 6. As shown, the mass values increase with the initial values. In addition, there is a lower bound for the mass values (the case of zero initial condition). From the vortex theory point of view, this phenomenon may be explained by the following argument: as the initial induced velocity is increased, the vortex segments are floating downstream away from the disc with higher velocity and create a larger angle relative to the disc plane. Thus, the mechanism that converts bound vorticity changes to induced velocity becomes slower which is equivalent to higher mass values. The conclusions drawn from this check is that the influence of the initial conditions is significant, however, it is bounded between well-defined limits.

To determine the equivalent mass sensitivity to various spanwise load distributions, three step function commands with zero initial conditions and different distributions were examined: 1) an "ideal" (constant) distribution, 2) an "approximate" (linear) distribution, and 3) a "realistic" (obtained from a steady blade-element-momentum theory) dis-

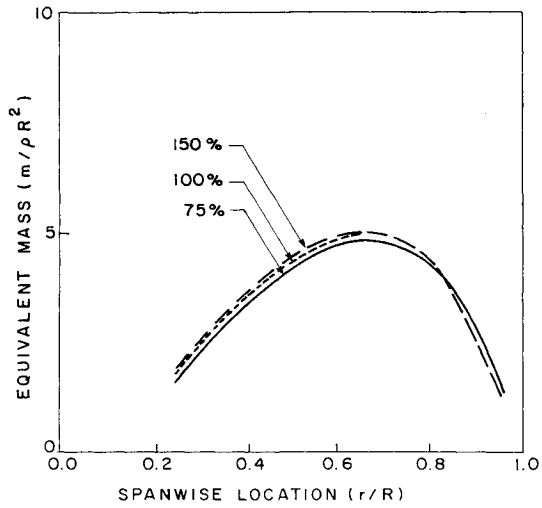

Fig. 5 Equivalent mass values for different end values of circulation.

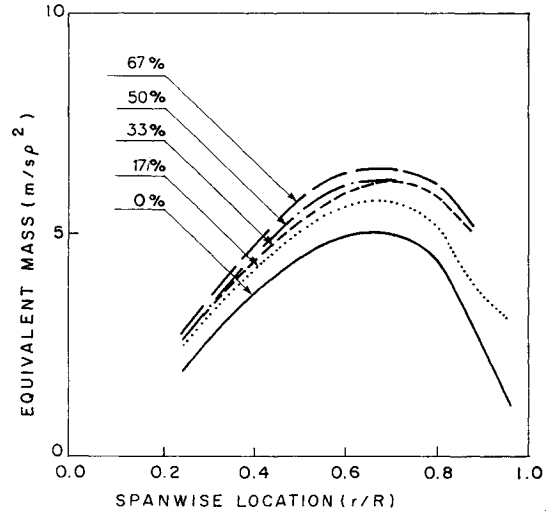

Fig. 6 Equivalent mass values for different initial values of circulation.

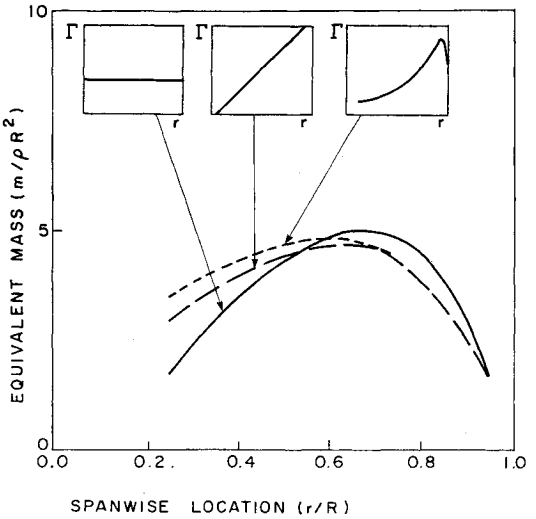

Fig. 7 Equivalent mass values for different spanwise load distributions.

tribution. The results are presented in Fig. 7 from which it is clear that as the spanwise load variations increase, the equivalent mass distribution becomes more uniform while the inboard regions show higher sensitivity.

Equations of Motion

System of Coordinates

As already mentioned, the present analysis deals with the response of a helicopter in hover and axial flight. Thus, it is convenient to choose a "fuselage" system of coordinates ($\hat{x}_F$, $\hat{y}_F$, $\hat{z}_F$) which is rigidly connected to the fuselage and parallel to the inertial system ($\hat{x}_I$, $\hat{y}_I$, $\hat{z}_I$) as shown in Fig. 8. The "hub" system of coordinates ($\hat{x}_H$, $\hat{y}_H$, $\hat{z}_H$) is connected to the rotor at the hub and rotates with it. Figure 5 also defines the azimuth angle ψ. In addition, a local "deformed" system of coordinates ($\hat{x}_D$, $\hat{y}_D$, $\hat{z}_D$) is attached to each cross section along the blade, while its orientation is determined by the three rotations in the lead-lag, flap, and torsion directions, respectively.

Degrees of Freedom

The present formulation includes elastic and rigid body degrees of freedom (DOF). The elastic DOF are the displacement in the flapwise direction (w), and its spanwise derivative (w_x), the displacement in the edgewise direction (v), and its spanwise derivative (v_x), and the elastic twist (ϕ) about the elastic axis (after the transverse displacements took place). The helicopter rigid body DOF are the rotor azimuth angle ψ, and the vertical position of its c.g., z_h (see Fig. 8). Since no axial DOF is included, an approximation of the radial motion due to the transverse displacements is utilized.

Structural Modeling

From a structural point of view, the blades are modeled as slender beams having arbitrary distributions of properties such as stiffness, mass, c.g. location, etc. By adopting the Bernoulli-Euler assumptions and assuming small strains and moderate elastic rotations, the elastic rotations due to v, w, and ϕ are defined as three Euler angles based on a second-order approximation.

Position Vector

The derivation of the equations of motion is based on the expressions for the position vector of each material point of

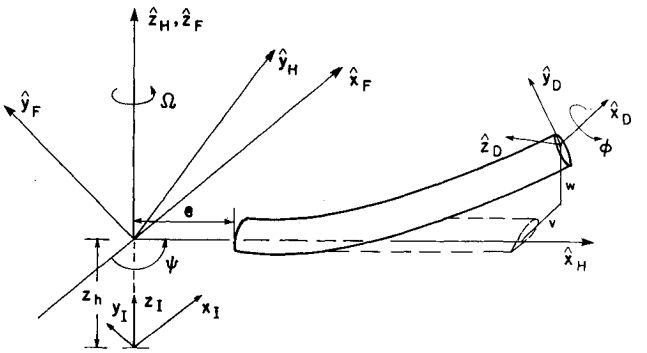

Fig. 8 Inertial, fuselage, hub, and deformed systems of coordinates.

the blade (located at x, y, z in the $\hat{x}_H$, $\hat{y}_H$, $\hat{z}_H$ directions before the deformation) in the inertial system as a function of time

$$\bar{R}_{(x,y,z,t)} = [T_{FH}]\left\{\begin{Bmatrix} e \\ 0 \\ 0 \end{Bmatrix} + \{X_e\} + [T_{HD}]\begin{Bmatrix} 0 \\ y \\ z \end{Bmatrix}\right\} + \begin{Bmatrix} 0 \\ 0 \\ z_h \end{Bmatrix} \tag{9}$$

where $[T_{FH}]$ is a transformation matrix that transforms a vector in the Hub system to its form in the Fuselage system, e is the blade offset (see Fig. 8), $\{X_e\}$ contains the elastic axis coordinates in the Hub system, y and z are the coordinates of a material point at each cross section, $[T_{HD}]$ is a transformation matrix that transforms a vector in the Deformed system to its form in the Hub system, and z_h is the vertical position vector (height) of the hub.

Proper differentiation of the position vector with respect to time enables one to express the kinetic energy and its derivatives as required for constructing the Lagrange equations of motion. It is important to note that all terms containing time derivatives were retained in these equations. This is essential in the present case of rapid time variations where time derivatives may change the terms' order of magnitude throughout the response. All analytical derivations were executed and coded using symbolic mathematical manipulation software.[12]

Finite Element Formulation

As already mentioned, the present solution is based on the finite element approach. Accordingly, the blade is divided into beam elements. For each element, the following vector of DOF has been assigned:

$$\{q_X\} = \langle w_L, w_{xL}, v_L, v_{xL}, \phi_L, w_R, w_{xR}, v_R, v_{xR}, \phi_R \rangle^T \tag{10}$$

where the indices L and R stand for the element left and right sides, respectively.

Time Integration

Assembling the contributions of all the elements results in a coupled system of equations which is replaced by two equivalent systems of equations so that a separation between the rigid and the elastic DOF is obtained. Consequently, the resulting equations of motion become

$$[M_{XX}]\{\ddot{q}_X\} + [K_{Xx}]\{q_X\} + [C_X]\{\dot{q}_X\} + \{N_X\} + [M_{XR}]\{\ddot{q}_R\} = \{Q_x\} \tag{11a}$$

$$[M_{RR}]\{\ddot{q}_R\} + [K_{RR}]\{q_R\} + [C_R]\{\dot{q}_R\} + \{N_R\} + [M_{XR}]^T\{\ddot{q}_X\} = \{Q_R\} \tag{11b}$$

where $[M_{IJ}]$, $[K_{IJ}]$, $[C_I]$, $[N_I]$ are mass matrices, stiffness matrices, damping matrices, and vectors of nonlinear contributions, respectively. $\{q_R\}$ contains the rigid DOF and is given by

$$\{q_R\}^T = \langle \psi, z_h \rangle \tag{12}$$

Each time step in the simulation is carried out as follows:

1) Initial values of $\{q_X\}$, $\{\dot{q}_X\}$, $\{q_R\}$, $\{\dot{q}_R\}$ are introduced.

2) The time-dependent terms in Eqs. (11a) and (11b) are determined.

3) The vector $\{\ddot{q}_R\}$ is determined by Eq. (11b).

4) The vector $\{\ddot{q}_R\}$ is substituted by Eq. (11a) from which the vector $\{\ddot{q}_X\}$ is obtained.

5) Since nonlinear expressions are involved, the above steps are repeated until convergence is achieved.

Once the values of $\{\ddot{q}_R\}$, $\{\ddot{q}_X\}$ are obtained and an integration step is performed, the above iterative procedure is repeated for the next time step.

Results

Based on the above aerodynamic and structural dynamic modeling, a code that simulates the time history of the involved DOF has been developed. The following is a summary of the parametric investigation and is based on a detailed description of the nominal case followed by successive variations of the main parameters. A full description of the above study may be found in Ref. 13.

Nominal Case

The nominal case is based on a typical full-scale hingeless rotor-fuselage system, the basic dimensions and parameters of which are presented in Table 1. The blades have uniform distribution of geometrical mass and stiffness properties and linear aerodynamic washout. Collective increase has been introduced by a "ramp" command of relatively high rate of 200 deg/s up to a constant value of 2 deg. In addition, in this nominal case, the helicopter is not allowed to move vertically (i.e., $z_h = 0$).

Thrust Response

Figure 9a describes the rotor aerodynamic thrust response (by a full line). As shown, the first peak has a "pointed" shape, then a sharp minimum is observed followed by a second overshoot peak, while the thrust at steady state is 34% higher than the initial one. Similar behavior may be found in Ref. 3 which is based on a vortex theory numerical scheme. Note that the aerodynamic thrust is obtained by integrating the aerodynamic loads along the blades span in the z_H direction and is only part of the total thrust that is transferred to the fuselage. Figure 9a also presents (by a dotted line) the total thrust acting on the fuselage which also includes dynamic loads. Comparison of the total and the aerodynamic thrusts demonstrates the important role of the dynamic response and reveals some interesting facts. First, the pointed peaks in the aerodynamic thrust has disappeared. Moreover, there is some lag in the total thrust at the initial response as opposed to a sharp rise of the aerodynamic thrust at that time. In addition, the total thrust is growing rapidly after this lag and reaches higher values than that of the aerodynamic thrust and in shorter time. These phenomena are the result of the elastic flapping motion which exhibits high acceleration and velocity values at the region under discussion. The blade mass, which is accelerated upwards, results in a downward force acting on the fuselage. This force is subtracted from the aerodynamic thrust and since its magnitude is almost equal to the aerodynamic force at the very beginning, the resulting load is very small. Following this initial response, the flapping motion is decelerated and the total thrust increases rapidly. The above phenomena is even more pronounced in the case of articulated blades.

Shaft Moment

Prior to the introduction of the collective pitch change, the axis moment in the z_H direction which is required for sustaining the rotational speed is determined. Then, assuming that during the blades response the rotational speed remains constant, Fig. 9b presents (by the full line) the additional (negative) aerodynamic shaft moment which is required to maintain the rotation. In contrast with the thrust behavior, this response has relatively low overshoot. This phenomenon results from the in-plane aerodynamic loads, and in particular, the induced drag which depends on aerodynamic lift. Downward flapping results in an increase in the angle of attack that also rotates the lift vector forward so that its in-plane components contribute to a decrease in the required moment. Figure 9b also presents (by the dotted line) the additional total moment needed for maintaining constant angular speed.

Table 1 Nominal case data

Number of blades	$N_B = 4$
Radius	$R = 7.3$ m
Chord	$c = 0.53$ m
Angular speed	$\Omega = 30.3$ rad/s
Built-in twist	$\theta_t = -1$ deg/m
Offset	$e = 0$
Cross-sectional area	$A = 3.2 \cdot 10^{-3}$ m^2
Mass per unit length	$m = 9.3$ kg/m
Cross-sectional stiffness and inertia properties	
Edgewise stiffness	$EIyy = 2.5 \cdot 10^6$ N·m^2 ($EIyy/m\Omega^2R^4 = 0.1$)
Flapwise stiffness	$EIzz = 5.0 \cdot 10^5$ N·m^2 ($EIzz/m\Omega^2R^4 = 0.02$)
Coupled stiffness	$EIyz = 0$
Torsional stiffness	$GJ = 5.7 \cdot 10^4$ N·m^2 ($GJ/m\Omega^2R^4 = 0.0024$)
Torsional inertia	$I_0 = 1.58 \cdot 10^{-2}$ kg·m ($= 2.5 \cdot 10^{-4} mR^2$)
Center of gravity location	$Ycg = 0$; $Zcg = 0$
Aerodynamic center location	$Yac = 0$; $Zac = 0$
Cross-sectional aerodynamic properties	
Lift curve slope	$a_0 = 5.7$ 1/rad
Drag coefficient	$C_d = 0.01$
Moment coefficient	$C_m = 0$
Fuselage weight	$w_F = 6.5 \cdot 10^5$ N
Motor moment of inertia	$I_M = 1000$ kg·m^2
Collective pitch rate	$\dot{\theta}_c = 200$ deg/s

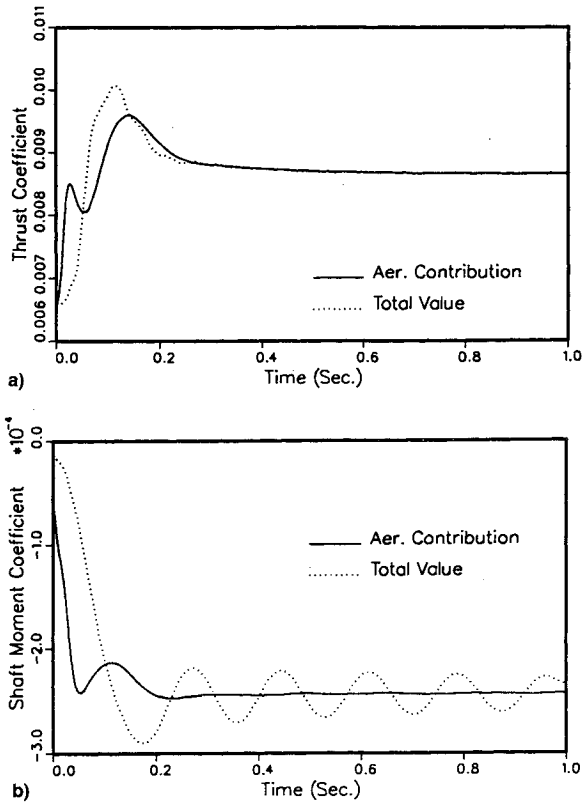

Fig. 9 Response of the aerodynamic contributions and the total values of the a) thrust and b) shaft moment (nominal case).

As shown, the total moment response is different from the aerodynamic moment response and reflects some lag and oscillations induced by the lead-lag motion. This behavior is a result of Coriolis loads which are created by the inward motion of the blade towards the rotation axis due to the flapping motion. These loads tend to reduce the required shaft moment at the initial response and are also dominant in the case of articulated blades.

Angle of Attack and Lift Distribution

The effective aerodynamic angle of attack shown in Fig. 10 is measured at the three-quarter chord location as required by the internal aerodynamic solution.[10] Note that this angle is the result of the collective pitch angle and its rate, the flapping motion velocity, and the helicopter climb velocity. As shown, for a command rate of 200 deg/s, the aerodynamic angle of attack responds relatively fast due to the high command rate that affects the angle of attack with no time delays. Subsequently, it is evident that the flapping velocity dominates the response. Later on, due to the development of the induced velocity, the angle of attack is slowly decreased towards its steady-state value.

Sensitivity Study

In what follows, a summary of a sensitivity study is presented. In each case, the nominal case has been perpetuated by changing only one of the parameters.

Command Rate

Different command rates have been examined from which it became obvious that this parameter has a notable influence. In the case of very slow command rate, the response of most of the parameters becomes almost monotonic having small overshoot, and the pointed peak that has characterized the aerodynamic angle of attack and thrust has disappeared, as shown for the angle of attack by Fig. 10. In addition, in the case of slow command rate, the induced velocity development is characterized by an initial lag followed by an almost linear increase until it settled down to a constant value.

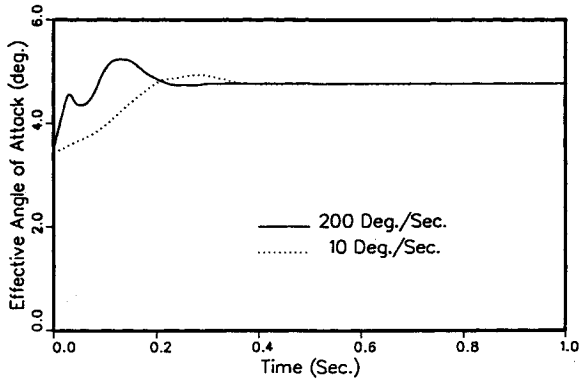

Fig. 10 Tip aerodynamics effective angle-of-attack response for 200 deg/s (nominal case) and for 10 deg/s.

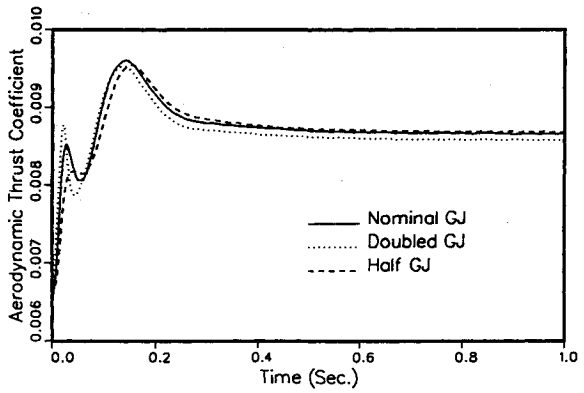

Fig. 11 Aerodynamic thrust response for different torsional stiffnesses.

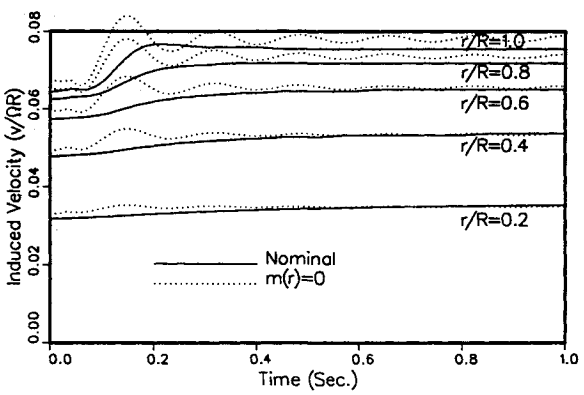

Fig. 12 Induced velocity response for vanishing equivalent mass values.

Torsional Stiffness

Figure 11 presents the aerodynamic thrust response for two different values of torsional stiffness of the blades—a half value and a double value of the nominal case, respectively. As shown, the torsional stiffness has a crucial influence on the pointed peak phenomena mentioned above with regard to the pitch rate contribution. However, the second overshoot is not sensitive.

Aerodynamic Equivalent Mass

Figures 12 and 13 present the induced velocity and thrust response, respectively, for vanishing values of the aerodynamic equivalent mass which represents no lag in the development of the trailing wake induced velocity. Note that the inner aerodynamic field still contains the unsteady effects. As shown, the induced velocity response is much more oscillatory in this case. Also, comparison of Figs. 9a and 13 shows that although oscillatory motion of the thrust is also observed for

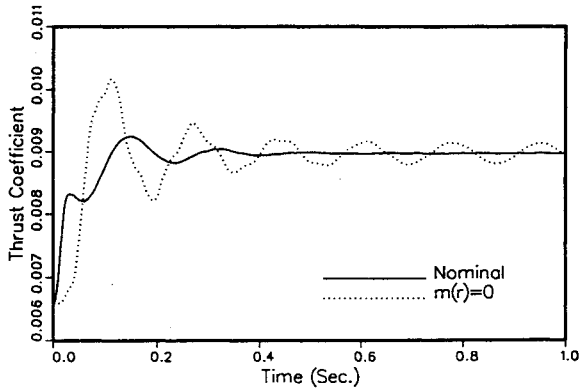

Fig. 13 Aerodynamic and total thrust response for vanishing equivalent mass values.

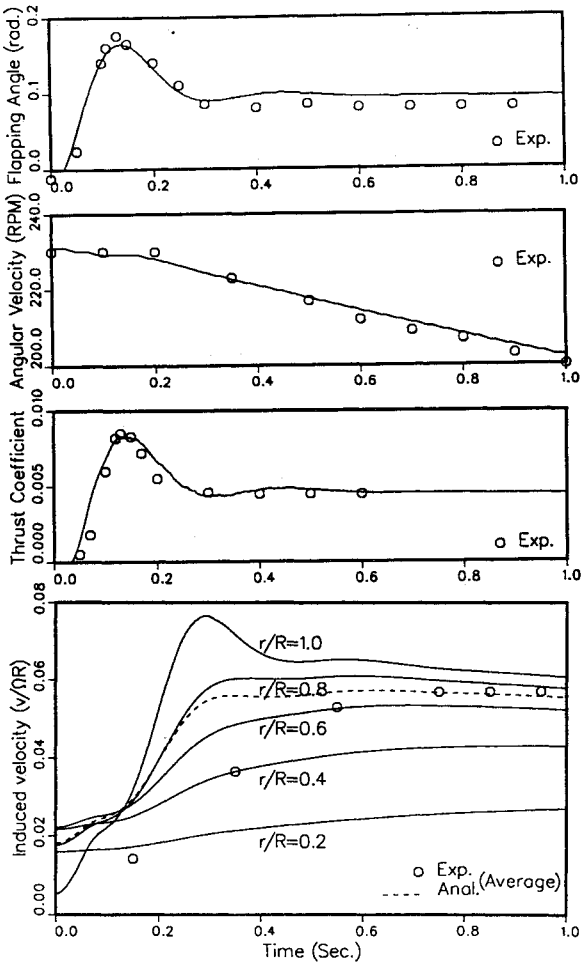

Fig. 14 Correlation with experimental data of Ref. 1 for articulated rotor (N_B = 3, R = 5.79 m, c = 0.254 m, Ω_0 = 24 rad/s, $\dot{\theta}_c$ = 200 deg/s, m = 4.71 kg/m).

vanishing values of the equivalent mass, the maximal thrust overshoot has not been changed.

Experimental Correlation

Correlations with experimental results presented by Carpenter and Fridovich[1] are presented in Fig. 14. In these experiments, articulated blades undergoing rapid variations in collective pitch angles were tested. Note that there are some uncertainties in the data concerning blade properties (e.g. and aerodynamic center locations, stiffnesses, etc.). Overall, the results presented in Fig. 14 for command rate of 200 deg/s demonstrate good correlation. The lag in the rotational speed decrease at the initial response which is induced by the shaft axis response (see Fig. 9b) is clearly observed in this case.

Concluding Remarks

Theoretical study of the response of helicopter blades to a sharp collective change in hover has been presented.

The three-dimensional, unsteady aerodynamic solution is based on the definition and determination of the distribution of equivalent aerodynamic mass. Parametric study has proved that this mass distribution has low sensitivity to most of the involved parameters and a priori determination of it is justified. The usage of these equivalent mass values for the calculation of the induced velocity response enables substantial saving of computational effort.

Combining the aerodynamic modeling with structural dynamic analysis of elastic blade, yielded some interesting observations.

1) In cases of rapid collective increase, the response is dominated by the dynamics of the elastic flapping motion which also creates notable differences between the aerodynamic thrust and the total thrust transferred to the fuselage.

2) There is a lag in the development of the required shaft moment response due to the rapid flapping response.

3) The command rate has a significant influence on the overshoot values of most parameters.

4) The equivalent mass was found to play an important role. However, the results sensitivity to small changes in its values was found to be smaller in cases of extremely rapid collective change since the induced velocity development is relatively slow and becomes influential only after the flapping motion has reached its maximal values.

5) Elastic effects were found to be important in hingeless blades due to their crucial influence on aerodynamic loads. In particular, a pointed peak in the aerodynamic loads development is clearly observed in blades having high torsional stiffness and disappear in blades that are soft in torsion.

References

[1]Carpenter, P. J., and Fridovich, B., "Effects of a Rapid Blade-Pitch Increase on the Thrust and Induced Velocity Response for a Full-Scale Helicopter Rotor," NACA TN 3044, Nov. 1953.

[2]Johnson, W., "Helicopter Theory," Princeton Univ. Press, Princeton, NJ, 1980.

[3]Segel, L., "Air Loadings on a Rotor Blade as Caused by Transient Inputs of Collective Pitch," U.S. Army Aviation Material Lab. TR 65-65, Oct. 1965.

[4]Quackenbush, T. R., "Computational Studies in Low Speed Rotor Aerodynamics," *Proceedings of the AHS National Specialists' Meeting on Aerodynamics and Aeroacoustics*, Arlington, TX, Feb. 25–27, 1987.

[5]Chen, R. T. N., "A Survey of Nonuniform Inflow Models for Rotorcraft Flight Dynamics and Control Applications," 15th European Rotorcraft Forum, Amsterdam, The Netherlands, Sept. 12–15, 1989.

[6]Bir, G., and Chopra, I., "Prediction of Blade Stresses Due to Gust Loading," *Vertica*, Vol. 10, Nos. 3/4, 1986, pp. 353–377.

[7]Rebont, J., Valensi, J., and Soulez-Lariviere, J., "Response of a Helicopter Rotor to an Increase in Collective Pitch for the Case of Vertical Flight," NASA Technical Translation F-55, June 1959.

[8]Pitt, D. M., and Peters, D. A., "Theoretical Prediction of Dynamic-Inflow Derivatives," *Vertica*, Vol. 5, No. 1, 1981, pp. 21–34.

[9]Chen, R. T. N., and Hindson, W. S., "Influence of Dynamic Inflow on the Helicopter Vertical Response," *Vertica*, Vol. 11, Nos. 1/2, 1981, pp. 77–91.

[10]Dinyavari, M. A. H., and Friedmann, P. P., "Unsteady Aerodynamics in Time and Frequency Domains for Finite Time Arbitrary Motion of Rotary in Hover and Forward Flight," AIAA Paper 84-0988, May 1984.

[11]Rand, O., and Rosen, A., "Efficient Method for Calculating the Axial Velocities Induced Along Rotating Blades by Trailing Helical Vortices," *Journal of Aircraft*, Vol. 21, No. 6, 1984, pp. 433–435.

[12]Seward, L. R., "Reduce User's Guide for IBM 360 and Derivative Computers," Version 3.3, The Rand Corp., Santa Monica, CA, July 1987.

[13]Hecht, Y., "Response of Helicopter Blades to a Sharp Collective Increase," M.S. Thesis, Faculty of Aerospace Eng., Technion—Israel Inst. of Technology, Haifa, Israel, 1990.